EINDHOVEN
UNIVERSITY OF
TECHNOLOGY

Characterization of ion emission of an extreme ultraviolet generating discharge produced Sn plasma

Citation for published version (APA):
Gielissen, K., Sidelnikov, Y., Glushkov, D., Soer, W. A., Banine, V. Y., & Mullen, van der, J. J. A. M. (2010). Characterization of ion emission of an extreme ultraviolet generating discharge produced Sn plasma. *Journal of Applied Physics*, *107*(1), 013301-1/7. Article 013301. https://doi.org/10.1063/1.3268462

DOI:
10.1063/1.3268462

Document status and date:
Published: 01/01/2010

Document Version:
Publisher's PDF, also known as Version of Record (includes final page, issue and volume numbers)

Please check the document version of this publication:

• A submitted manuscript is the version of the article upon submission and before peer-review. There can be important differences between the submitted version and the official published version of record. People interested in the research are advised to contact the author for the final version of the publication, or visit the DOI to the publisher's website.
• The final author version and the galley proof are versions of the publication after peer review.
• The final published version features the final layout of the paper including the volume, issue and page numbers.

Link to publication

General rights
Copyright and moral rights for the publications made accessible in the public portal are retained by the authors and/or other copyright owners and it is a condition of accessing publications that users recognise and abide by the legal requirements associated with these rights.

• Users may download and print one copy of any publication from the public portal for the purpose of private study or research.
• You may not further distribute the material or use it for any profit-making activity or commercial gain
• You may freely distribute the URL identifying the publication in the public portal.

If the publication is distributed under the terms of Article 25fa of the Dutch Copyright Act, indicated by the "Taverne" license above, please follow below link for the End User Agreement:

www.tue.nl/taverne

Take down policy
If you believe that this document breaches copyright please contact us at:

openaccess@tue.nl

providing details and we will investigate your claim.

Download date: 17. Nov. 2023

Characterization of ion emission of an extreme ultraviolet generating discharge produced Sn plasma

K. Gielissen,[1,a)] Y. Sidelnikov,[2] D. Glushkov,[3] W. A. Soer,[4] V. Banine,[3] and J. J. A. M. v. d. Mullen[1]
[1]*Eindhoven University of Technology, Den Dolech 2, 5600 MB Eindhoven, The Netherlands*
[2]*ISAN Institute of Spectroscopy, Fizicheskaya Str. 5, Troitsk, Moscow Region 142190, Russia*
[3]*ASML, De Run 6501, 5504 DR Veldhoven, The Netherlands*
[4]*Philips Research, High Tech Campus 4, 5656 AE Eindhoven, The Netherlands*

(Received 11 June 2009; accepted 3 November 2009; published online 4 January 2010)

The ion emission of a Sn-based discharge produced extreme ultraviolet producing plasma is characterized with the combined use of different time-of-flight techniques. An electrostatic ion spectrometer is employed to measure the average charge distribution of the emitted Sn ions. A dedicated Faraday cup configuration is used to measure the total ion flux from the source for different discharge energies. High-energy Sn ions emitted by the plasma with energies up to 100 keV have been identified. The number of high-energy ions increases for higher electrical input energy into the plasma while the signal associated with the expanding plasma ions does not show such dependence. The ion energy distribution for a bulk of detected ions is calculated based on the Faraday cup measurements and compared with theoretical plasma expansion dynamics. © *2010 American Institute of Physics*. [doi:10.1063/1.3268462]

I. INTRODUCTION

To reduce feature size in the semiconductor industry, future lithography tools will have to decrease the imaging wavelength. It is expected that lithography using extreme ultraviolet (EUV) radiation will be introduced to produce features smaller than 32 nm. EUV technology will make use of plasma sources, which produce EUV radiation to project small-scale patterns onto wafers. These sources have to produce sufficient EUV.[1] In alpha-level EUV exposure tools, sources based on a discharge produced plasma (DPP) of Sn have so far shown the highest EUV power.[2–4] In addition to the desired EUV radiation, however, these sources produce a significant amount of debris that can damage the collector optic. The lifetime of the collector optic in the source-collector assembly is one of the main challenges for EUV lithography to have high productivity.[5] In addition to Sn deposition, a major factor that determines the lifetime is ion sputtering of the material at the collector surface. These ions are produced by the plasma itself and it is important to understand the mechanisms that are responsible for the creation of these ions.

Previously, the ion emission from plasma based EUV sources has been investigated. It was found that DPP sources emit Sn ions with energies up to several tens of keV while for laser produced plasma sources the energy is limited to about 10 keV.[6–8]

This paper focuses on the characteristics of the ionic debris emitted by a Sn-based DPP source. The experiments are based on time-of-flight (TOF) velocity measurements of the ions performed with two different analysis tools. (1) An electrostatic spectrometer, which detects only ions for a chosen energy-to-charge ratio, is employed to measure the velocity of the ions. The energy-to-charge ratio in combination with the velocity allows identifying the ion species and the ion charge Z. (2) A dedicated Faraday cup (FC) configuration is used to measure a total ion flux as a function of time. Using the mean ion charge Z the total number of ions emitted by the discharge plasma is calculated. Then, the ion energy distribution (IED) emitted by the discharge plasma is determined using the TOF as a measure of the kinetic energy. Finally, a model based on the collisionless expansion of plasma into vacuum is employed to estimate the IED based on the plasma conditions during the pinch phase.

II. EXPERIMENTS

A. DPP source

A Sn-based DPP source developed at the Russian Institute of Spectroscopy (ISAN) is employed to study the ionic debris emission. The source consists of two closely spaced metal electrodes that rotate through a bath of liquid Sn. This keeps their surface continuously covered with a layer of liquid Sn so that electrode erosion is prevented.

Figure 1 shows a schematic of the source. Before the ignition of the discharge, a potential of about 4 kV is applied across the discharge gap ($\sim$3–4 mm) with the use of a capacitor bank. Next, a laser pulse evaporates liquid Sn from the cathode surface and a partly ionized Sn vapor expands to the anode. When the density near the anode is sufficiently high the discharge is initiated. This is typically about 100 ns after the laser pulse. The current through the discharges increases rapidly ($\sim$100 ns) and due to the Lorentz forces the plasma is compressed in a radial direction, thus creating a multiply ionized Sn plasma. The EUV radiation is emitted by one or more micropinches that subsequently develop in high Z plasmas according to the radiative collapse theory.[9] Finally the micropinch expands into vacuum and decays. The ob-

a)Electronic mail: k.gielissen@tue.nl.

 © 2010 American Institute of Physics

Downloaded 27 Apr 2010 to 131.155.108.152. Redistribution subject to AIP license or copyright; see http://jap.aip.org/jap/copyright.jsp

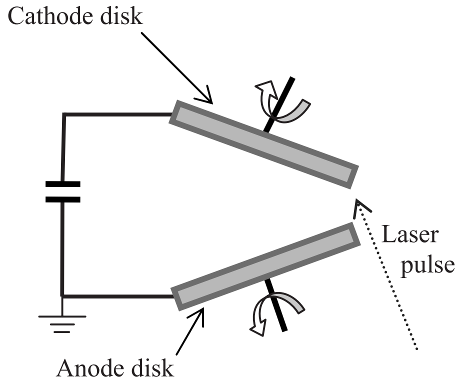

FIG. 1. Schematic top view of the DPP source. Two rotating disk electrodes are covered with a layer of liquid Sn. A laser pulse is used to evaporate the liquid Sn in between the electrodes, initiating the discharge.

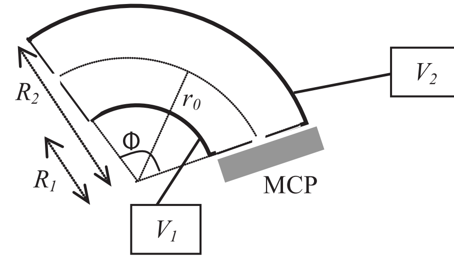

FIG. 2. Schematic of the electrostatic spectrometer based on the design of Hughes and Rojansky (Ref. 13). Two cylindrical surfaces having radii of curvature R_1 and R_2 are maintained on potentials V_1 and V_2. The angle Φ between the entrance slit and the exit slit equals to 127.3°. The particles that exit the spectrometer are detected using a MCP detector, read out by an oscilloscope.

served lifetime of a single micropinch in DPP sources equals about 10 ns. The typical plasma characteristics during the discharge were intensively studied on a similar source and can be found in Refs. 10 and 11. As the high density plasma is only short lived, the moment the micropinch develops will serve as a zero point on the time scale when performing TOF analysis of the ionic debris. It can be identified because of the high radiation emission or a sudden decrease in the discharge current.

The source is operated in a vacuum environment at a repetition frequency of 10 Hz and a discharge energy of $E_d = 4$ J/pulse. By changing the voltage applied to the capacitor bank E_d can be altered. A Nd:YAG (yttrium aluminum garnet) laser operating at a wavelength of 1064 nm is used to evaporate the liquid Sn in between the electrodes and thus trigger the discharge. The laser pulse has a time width of about 15 ns and a pulse energy of about 10 mJ. During the experiments presented in this paper, the detectors are positioned perpendicular to the discharge axis.

In Sec. II B an electrostatic spectrometer is described that is utilized to measure the ion charge distribution. Then, a dedicated FC configuration is described and the equation for calculating the IED from the cup signal is derived. With the FC the total ion flux emitted by the DPP source is measured and from this the IED is determined. Finally, a model describing the collisionless expanding plasma dynamics is used to estimate the IED based on the initial plasma properties.

B. Ion charge distribution

The electrostatic cylindrical spectrometer utilized in this experiment was constructed at ISAN,[12] and is based on the design of Hughes and Rojansky.[13] The parameters for optimum performance of this type of spectrometer have been calculated and measured previously.[14–17] Figure 2 shows a schematic of the spectrometer. Two cylindrical surfaces having radii of curvature $R_1 = 2$ cm and $R_2 = 3$ cm are placed between an entrance and an exit slit of width 0.5 mm and height 10 mm. The cylindrical surfaces are maintained at potentials V_1 and V_2, thus creating a potential difference of $\Delta V = V_1 - V_2$ between them. This potential difference produces an electrical field $F(r)$ inside the spectrometer. Charged particles entering the spectrometer will travel a circular path under the influence of the electric field. For each voltage ΔV, only ions with a specific energy-to-charge ratio will arrive at the exit slit and are detected using a multichannel plate (MCP) detector. The time-resolved detection of the MCP by means of an oscilloscope provides a TOF analysis.

An explanation of the working principle follows next, together with the derivation of the equation, which is employed to calculate the energy-to-charge ratio of the ions exiting the spectrometer. The equation of the electric field inside the spectrometer for $R_1 < r < R_2$ is as follows:

$$F(r) = \frac{\Delta V}{r \times \ln(R_2/R_1)}. \tag{1}$$

If an ion with mass m_i, speed v, and charge q enters the spectrometer, it will travel a circular trajectory with radius r because of the centripetal force acting on it. The following force equation must hold $m \times v^2/r_0 = q \times F(r_0)$ for ions passing through the exit slit of the electrostatic spectrometer. From Eq. (1) it follows that for these ions the following equation is valid: $E/q = \Delta V/[2 \times \ln(R_2/R_1)]$ where E is the kinetic energy. The charge q of the ion can be written as $Z \times e$ with Z the charge number and e the elementary charge. Now, for a spectrometer with $R_1 = 20$ mm and $R_2 = 30$ mm, this can be simplified to

$$E/Z = 1.23 \times e \times \Delta V \quad (\text{eV}). \tag{2}$$

From the TOF analysis the kinetic energy E of a detected ion can be calculated using

$$E_{\text{kin}} = \frac{m_i}{2} \times \left(\frac{D}{t}\right)^2, \tag{3}$$

where D is the distance from the spectrometer to the plasma and t is the TOF. Thus, by measuring the TOF of the detected ions, the ion species and charge number Z can be determined using Eqs. (2) and (3).

1. Experiment

A picture of a typical oscilloscope measurement of the spectrometer placed at a distance $D = 85$ cm from the plasma source is shown in Fig. 3. The division on the time scale equals 1 μs. Three traces can be seen: trace A represents the laser pulse igniting the discharge and trace B shows the time derivative of the discharge current. The time of the pinch is

Downloaded 27 Apr 2010 to 131.155.108.152. Redistribution subject to AIP license or copyright; see http://jap.aip.org/jap/copyright.jsp

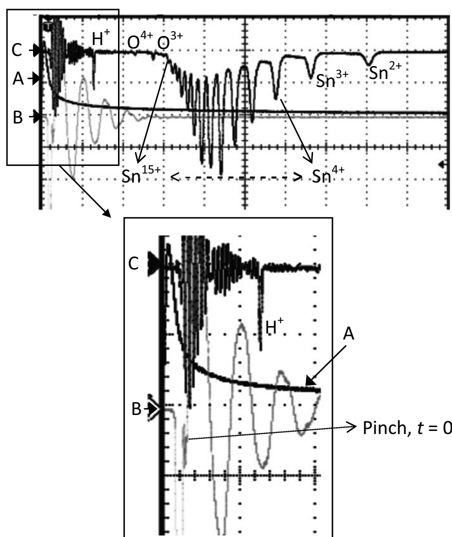

FIG. 3. A typical oscilloscope image of the measurement with the spectrometer. Trace A represents the laser pulse igniting the discharge, trace B shows the time derivative of the discharge current, and trace C gives the signal of the ion spectrometer for an E/Z value of 3.7 keV. The charges of the Sn ions of $Z=2$ up to $Z=15$ are visible. At the start of the signal some noise can be seen.

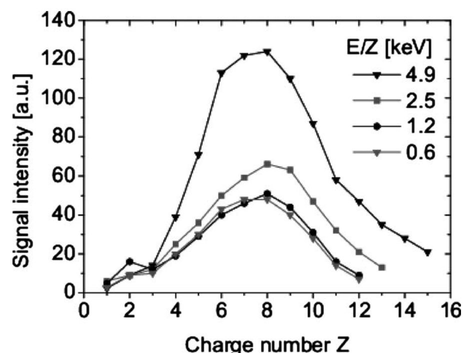

FIG. 4. The intensity of the Sn ion peaks from the spectrometer selection for different E/Z values are shown as a function of the charge number Z. The weighted average charge number for low E/Z values equals $Z=7$ and for high E/Z equals $Z=8$.

indicated by the arrow on the image magnification and is taken as zero on the time scale when performing TOF analysis. Trace C gives the spectrometer signal for $\Delta V=3$ kV as a function of time. From Eq. (2) it follows that only ions with $E/Z=3.7$ keV are detected. At the beginning of trace C, a large noise signal is visible during the time of the pinch followed by some small peaks from light elements. Apparently these are contaminants present in the plasma fuel. From TOF analysis and using Eq. (3) it is concluded that the main peaks observed in trace C are from Sn ions with charges $Z=2$ up to $Z=15$. The contaminants can be identified as H^+, O^{4+}, and O^{3+}.

For a given E/Z value, the detected contaminants have higher velocities than the Sn ions, and because they have a relatively low charge number, the contaminants have a lower kinetic energy than the highly charged Sn ions. As an example, the O^{4+} ion has a velocity of 4.3×10^5 m/s while its energy equals to 15 keV in comparison with the Sn^{15+} ion, which has a velocity of 3.0×10^5 m/s and an energy of 57 keV.

From Fig. 3 an estimate of the relative amount of contaminants with respect to the Sn ions can be made. When the ion impact energy is sufficiently high (>3 keV) heavy ions and low mass ions are detected with equal detection efficiency.[18–20] From this it follows that the signal intensity of ions of different species can be compared. However, because the detection efficiency may differ for particles with different kinetic energies, only the signal of ions with equal energy and $E_{\text{kin}}>3$ keV can be analyzed. A comparison from the peak intensity of the oxygen with the Sn ions for equal kinetic energy, e.g., O^{+4} and Sn^{+4} with $E_{\text{kin}}=15$ keV, shows that Sn is about eight times more abundant than oxygen.

We will now mainly concentrate on the Sn ions. In order to measure the average charge number for different energy ranges of the emitted ionic debris, the spectrometer signal is recorded for various values of ΔV. The intensity of the Sn ion peaks from the spectrometer measurement are shown versus the charge number Z in Fig. 4 for various values of E/Z. The increase in signal intensity for higher E/Z values should not be interpreted as a larger number of ions; as will be shown later the number of high-energy ions is much less than that of the low-energy ions. The number of ions emitted by the source will be measured as a function of time with the FC in Sec. II C. Figure 4 shows that for lower ion energies ($E/Z=0.6$ keV) the weighted average charge equals to $Z=7$ and for higher ion energies ($E/Z=4.9$ keV) the average charge number equals to $Z=8$.

The kinetic energy of the ions can be calculated by multiplying the charge number by the corresponding E/Z value. The energy detected is from the $E/Z=4.9$ keV series; these ions have a velocity of 3.5×10^5 m/s, which corresponds to an energy of $E_{\text{kin}}=74$ keV for the Sn ions with charge number $Z=15$. This maximum in the measured energy is because of the voltage limit of the spectrometer. A higher voltage at the deflection plates could damage the interior electric components. It is expected that Sn ions with higher energies can be found among the debris.

Concluding, these experiments indicate that the high velocity ionic debris not only consists of high-energy Sn ions but of high velocity contaminants such as H^+, O^{3+}, and O^{4+} as well. It is shown that the Sn ions can have energies up to 74 keV. The electrostatic spectrometer, however, is unable to detect higher energies due to the apparatus limit. Furthermore, no information about the number of ions can be deduced from these results.

In Sec. II C a dedicated FC detector is employed. This detector not only allows measuring the ion flux as a function of time, but also has no limiting operation voltage for the detection of ions.

C. IED

FC detectors are commonly utilized for the investigation of the ion flux from plasmas.[21,22] These detectors are commercially available[23] but are often homemade as specific conditions demand for a dedicated configuration. The working principle of a FC is as follows: The cup is positioned at

Downloaded 27 Apr 2010 to 131.155.108.152. Redistribution subject to AIP license or copyright; see http://jap.aip.org/jap/copyright.jsp

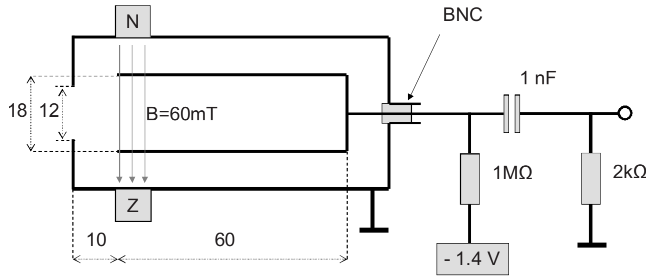

FIG. 5. Schematic of the dedicated FC detector configuration. The cup has a length of 60 mm and a diameter of 18 mm. In order to repel external secondary electrons it is biased with a voltage of −1.4 V. A magnetic field, with a field strength of $B=60$ mT at the center of the cup, is used to prevent internal secondary electrons from exiting the cup. The current through the load resistor $R=2.0$ kΩ is a measure of the captured ions.

a certain distance D from the plasma and the collected charge is measured as a function of time. For a good configuration, the charge is a measure for the number of ions that are captured by the cup per unit of time. From the average charge number Z_{av} measured in Sec. II B, the total ion flux can be calculated. With the use of the TOF of the ions, their kinetic energy is determined and the IED is calculated.

In order to perform energy analysis of the captured ions or to suppress electrons from escaping the cup, a repelling grid is frequently employed. This grid is placed in front of the cup and may be negatively biased to prevent the escape of secondary electrons out of the cup or positively biased for ion energy analysis. However, the use of a grid as an energy analysis tool can introduce unwanted space charge effects in front of the cup.[24,25] Furthermore, when measuring the ion flux of EUV producing plasmas with a FC, one has to be aware of two mechanisms that can disturb the measurement.

First, the emitted plasma radiation creates secondary electrons by impact on metal surfaces. These surfaces not only include the vacuum chamber walls but the FC surface as well. In view of the fact that the energy of the detected ions is calculated with the TOF technique, a large signal during the discharge cycle may prohibit the detection of high-energy ions arriving at the cup shortly after the pinch. Such a signal can be produced because of secondary electrons from the walls entering the FC and thus creating a negative signal, or from secondary electrons escaping the FC and creating a positive signal.

Second, the impact of high-energy ions on surfaces will also produce secondary electrons. This may lead to a signal increase or signal decrease. If an ion is collected inside the cup and secondary electrons escape, the signal will increase and it will appear as if more ions were detected. The signal will decrease when ions collide with the vacuum chamber walls near the FC and the secondary electrons are collected with the cup.

Concluding, the production of secondary electrons, either by radiation or by high-energy ions, in or nearby the FC has to be prevented. Thus the presence of a grid in front of the FC is not favorable. In order to obtain a low noise signal and optimal detection efficiency a dedicated FC configuration has been developed. Figure 5 shows the schematic of the FC detector.

The cup is made of a thin copper foil and has a length of 60 mm, a diameter of 18 mm, and is connected to a coaxial BNC connector. An aperture of 12 mm is placed in front of the cup to prevent radiation or ions from reaching the vacuum chamber walls near the cup in the case of a small beam misalignment. In order to repel the secondary electrons from the chamber walls the cup is biased with a voltage of −1.4 V. With the use of permanent magnets placed outside the vacuum, a magnetic field is created at the FC entrance to prevent secondary electrons from escaping the cup. The magnetic field strength at the center of the cup equals 60 mT. The charge collected by the cup is measured as the voltage $V(t)$ across the load resistor $R=2.0$ kΩ as a function of time.

When the cup is aligned correctly electrons and photons are of no influence and the collected charge is solely the result of a number of ions n_i transmitted through the limiting aperture and captured by the cup. Now a derivation follows to calculate the total ion flux dN/dt and the IED dN/dE using the charge $Q(t)$ collected by the FC as a function of time.

From Ohm's law it follows that for the charge $Q(t)$ collected by the cup the following equation holds:

$$\frac{dQ}{dt} = \frac{V(t)}{R}, \tag{4}$$

where $V(t)$ is the measured voltage across the load resistor R at a time t after the pinch. Assuming that the charge $Q=n_i \times e \times Z_{av}$ collected by the cup is solely due to the capturing of n_i ions with average charge number Z_{av} we can write Eq. (4) as

$$\frac{dn_i}{dt} = \frac{V(t)}{e \times Z_{av} \times R} \tag{5}$$

with dn_i/dt the number of ions collected by the FC per unit of time. Now, if a limiting aperture with diameter d in front of the FC is positioned at a distance L from the plasma then the total ion flux per unit of time dN/dt is equal to

$$\frac{dN}{dt} = \frac{V(t)}{e \times Z_{av} \times R} \times (2 \times \pi \times L^2) \times \left(\frac{\pi \times d^2}{4}\right)^{-1}. \tag{6}$$

This can be converted to the IED using $dN/dE = dN/dt \times dt/dE$. Here dt/dE can be replaced with $-2 \times E/t$ since Eq. (3) gives the expression for the kinetic energy E. This leads to the following expression for the IED:

$$\frac{dN}{dE} = -\frac{8 \times V(t) \times L^2 \times t^3}{e \times Z_{av} \times R \times m_i \times D^2 \times d^2}. \tag{7}$$

By integrating Eq. (7) for a certain range of energy, one can calculate the number of ions in the interval having these energies and emitted by the source in a solid angle of 2π.

1. Experiment

For the measurement of the ion flux emitted by the DPP source, the FC is mounted to the source chamber at a distance $D=100$ cm from the plasma, perpendicular to the discharge axis. An additional aperture with diameter $d=2$ mm is placed at a distance $L=18$ cm from the plasma in front of the FC. In this way a small misalignment of the FC entrance

Downloaded 27 Apr 2010 to 131.155.108.152. Redistribution subject to AIP license or copyright; see http://jap.aip.org/jap/copyright.jsp

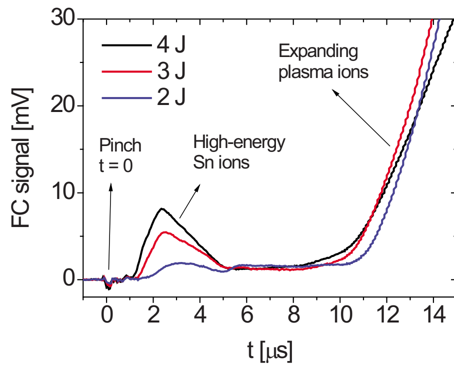

FIG. 6. (Color online) The averaged FC signal measured as a function of time for E_d=2 J, E_d=3 J, and E_d=4 J. The negative signal right in the beginning is because of collected electrons at the time of the pinch, and is taken as zero on the time scale.

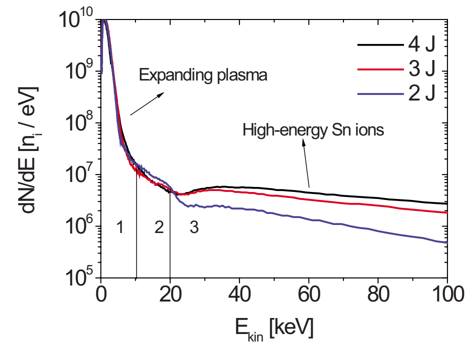

FIG. 7. (Color online) The IED dN/dE calculated from the FC signal using Eq. (7) shown as a function of E_{kin}. For the calculation it is assumed that all detected particles are Sn ions and kinetic energies >100 keV are not shown.

to the ion beam will not result in an additional production of secondary electrons. It should be noted that the limiting aperture locally introduces a space charge that suppresses the number of ions being transmitted by the aperture. Although the aperture partially suppresses the signal, this configuration allows a better analysis of the FC signal. Because of a substantial variation of the pulse-to-pulse FC signal it is chosen to measure the average ion flux over a number of consecutive pulses. Figure 6 shows the FC signal as a function of time for E_d=2 J, E_d=3 J, and E_d=4 J.

The negative signal seen at the beginning of the FC trace is the result of the collection of secondary electrons. These are produced in the vicinity of the cup during the time of the pinch. This is taken as zero on the time scale. At a time of 1–5 μs after the pinch, a *beam* of ions is measured with the FC. These ions have high velocities and thus are highly energetic. The positive signal at about 8 μs is expected to be the result of the collection of normal Maxwellian ions from the expanding Sn plasma. It can be clearly seen that the discharge energy of the plasma has a large influence on the emission of high-energy ions but for $t>5$ μs no significant change is observed in the FC signal. The expanding plasma seems to be unaffected by the discharge energy.

TOF analysis shows that the ions from the expanding plasma have velocities up to 1.3×10^5 m/s, which corresponds to E_{kin}=10 keV for the case of Sn ions. The high-energy ion beam consists of ions with velocities in the range of 1.0×10^6 to 2.0×10^5 m/s. In Sec. II B it is shown that in this range of velocities not only high-energy Sn ions but also contaminants are present. Thus the *peak* signal will be the result of the collection of a combination of different ion species. It is not possible to identify them solely with the FC data and therefore an estimate of the contribution of the Sn ions to this *peak* signal will be made using the results from the experiments with the spectrometer.

The maximum measured velocity of Sn ions in Sec. II B is 3.5×10^5 m/s; this equals to E_{kin}=74 keV, and this was only limited by the maximum voltage ΔV of the spectrometer. Oxygen ions with velocities up to 4.3×10^5 m/s were also detected as shown in Fig. 3. However, a highly charged Sn ion contributes more to the charge Q collected by the FC than a lowly charged contaminant. Moreover, the results of the spectrometer suggest that Sn ions are much more abundant than contaminants as mentioned above. Therefore it is reasonable to suggest that the Sn ions can have velocities up to 4.0×10^5 m/s, which corresponds to E_{kin}=100 keV, and that these high-energy Sn ions contribute to the major part of the *peak* signal from Fig. 6. It is not to be excluded that even higher energetic Sn ions are present in the high-energy ion beam. In order to verify this, however, experiments with an electrostatic spectrometer have to be performed where deflection voltages in the range of tens of kilovolts can be applied.

Now with the use of the average ion charge Z_{av} measured in Sec. II B, the setup parameters, and the FC data from Fig. 6, the IED dN/dE emitted in a solid angle of 2π can be calculated using Eq. (7). For the calculation it is assumed that all ions collected with the cup are Sn ions and that the ion emission is isotropic. Actual ion emission may be anisotropic; thus the calculation presented below may differ several times from actual emitted ion flux in a specific direction. Figure 7 shows dN/dE as a function of E_{kin} for different E_d values. The trace can be divided into three different parts.

(1) The low-energy part ($E_{kin}<10$ keV) was found to be similar for the different discharge energies and resembles Maxwellian energy distribution, as will be shown later. This part is expected to be the result of the expansion of the plasma into vacuum after the discharge. By integrating this signal it follows that approximately 10^{14} ions are emitted in 2π by the source with E_{kin} <10 keV. A typical plasma column[11] with radius R_0 =0.5 mm, a height of 3 mm, an average electron density of $n_e=1\times10^{24}$ m^{-3}, and considering an average ionization number of Z=8 consists of about 3×10^{14} ions. This shows that the number of ions emitted by the source is of the same order of magnitude as the total number of ions inside the initial plasma column. The discharge plasma is thus fully ejected into vacuum after the pinch phase.

(2) The second part of the IED (10 keV<E_{kin}<20 keV) has a different slope and also does not change with E_d. This part is calculated out of the FC signal trace for 5 μs<t<8 μs from Fig. 6. This part of the FC signal is constant in time but nonzero and therefore contributes

Downloaded 27 Apr 2010 to 131.155.108.152. Redistribution subject to AIP license or copyright; see http://jap.aip.org/jap/copyright.jsp

to the IED. Possibly it is a transition region between the two main signals or it may be the sum of the tails of the two signals that overlap each other.

(3) The third part ($20\ \text{keV} < E_{\text{kin}} < 100\ \text{keV}$) represents the high-energy ion beam consisting of Sn ions that are clearly not part of the expanding plasma plume. This part of the signal changes for different discharge energies. The ions most likely result from different mechanisms that can produce suprathermal particles.[26] These mechanisms may include the formation of anomalous resistivity and high inductive voltages during the current breakup after the pinch. It appears that an increased E_d enhances the formation of high-energy ions.

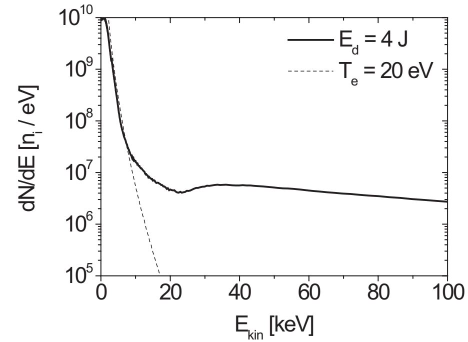

FIG. 8. The measured IED dN/dE for E_d=4 J is shown together with the calculated dN/dE from Eq. (8) as a function of E_{kin}. As input parameters T_e=20 eV, n_e=1×10^{24} m^{-3}, and R_0=100 μm.

III. PLASMA EXPANSION INTO VACUUM

In this section, an analytical model is used to calculate the IED of the expanding plasma using parameters from the initial plasma conditions. This model will be compared with the previous measurement for E_d=4 J. For a collisionless plasma that expands into vacuum, the charge separation effects have been studied intensively.[27] It is assumed that at $t=0$, the plasma occupies the half space $x<0$ and consists of cold ions that are initially at rest and of electrons, with temperature T_e and number density n_e that obey Boltzmann statistics. When the plasma expands, the ion movement is described with the equations of continuity and motion. A self-consistent solution can be found if one assumes quasineutrality in the expanding plasma. This leads to an IED of the following form:[27]

$$\frac{dN}{dE} = \frac{S \times n_{i0} \times c_s \times t}{\sqrt{2 \times E \times Z_{\text{av}} \times T_e}} \exp\left(-\sqrt{\frac{2 \times E}{Z_{\text{av}} \times T_e}}\right), \tag{8}$$

where E is the kinetic energy of the ions, $n_{i0}=n_e/Z_{\text{av}}$ the initial (planar) ion density, and S is the surface with radius R_0 of the initial plasma. The ion acoustic velocity c_s is given by $c_s=(Z\times T_e/m_i)^{1/2}$.

With the use of Eq. (8) the IED of the expanding Sn plasma is calculated. For this an average ionization number of $Z_{\text{av}}=8$ is assumed, the electron density of a typical plasma column is used[11] $n_e=1\times10^{24}$ m^{-3}, and the radius $R_0=100$ μm is based on the equilibrium radius of the pinch estimated with the radiative collapse theory.[28] The plasma temperature T_e is used as a fit parameter. Figure 8 shows the result of the calculation with Eq. (8) for T_e=20 eV together with the measured IED for E_d=4 J. This value of T_e is experimentally confirmed.[11]

For $E_{\text{kin}}<15$ keV the model nearly coincides with the measurement. This shows that the electron temperature of T_e=20 eV closely resembles the temperature of the initial plasma from where the ions originate. For $E_{\text{kin}}>10$ keV, however, the measured IED starts to differ from the model calculations.

First, for $10\ \text{keV} < E_{\text{kin}} < 20\ \text{keV}$, it appears that the tail of the Maxwell distribution has increased. As discussed in Sec. II, this possibly is a transition regime between the expanding plasma and the high-energy ion beam. Then, for $E_{\text{kin}}>20$ keV, the high-energy ion beam is clearly not part of the expanding plasma ions as predicted by the model. The high-energy ions are expected to be the result of plasma instabilities during the discharge that can produce suprathermal ions.[26]

The production mechanisms of these high-energy ions are beyond the scope of this paper. It should be noted that these plasma instabilities are typical for pinch plasmas but their formation is not unavoidable. If sufficient understanding is gained from the formation of these instabilities, measures can be taken to suppress the production of the high-energy ion beam and thus increase the lifetime of collector optics in DPP EUV sources.

IV. CONCLUSION

An electrostatic ion spectrometer is utilized to measure the charge distribution of the emitted Sn ions. Although the spectrometer is limited to measure ions with a maximum E/Z value of 4.9 kV, Sn ions with charge Z=15 and kinetic energy up to 74 keV are identified. The average charge of the Sn ions collected by the detectors is found to equal Z_{av}=8.

A dedicated FC configuration is employed to measure the ion flux as a function of time for different plasma discharge energies. TOF analysis of the FC signal allowed the determination of the IED. This distribution is compared with the result of an analytical model describing the collisionless expansion of a plasma into vacuum. For these calculations isotropic ion emission is assumed. As pointed out above, the actual ion emission may be anisotropic and the presented calculations may differ several times from the actual emitted ion flux in a specific direction.

It is shown that the measured IED consists of two important parts. The low-energy part ($E_{\text{kin}}<10$ keV) has a Maxwellian distribution and is described by the plasma expansion model using an initial electron temperature of $T_e=20$ eV. The second part for $E_{\text{kin}}>20$ keV consists of suprathermal Sn ions with energies up to 100 keV. An increase in the plasma discharge energy enhances the high-energy ion emission, while the ions from the expanding plasma are hardly affected.

The mechanisms that can lead to the suprathermal Sn ion production are beyond the scope of this paper. Several mechanisms for high-energy ion production, such as anomalous resistivity and high inductive voltages during the current

Downloaded 27 Apr 2010 to 131.155.108.152. Redistribution subject to AIP license or copyright; see http://jap.aip.org/jap/copyright.jsp

breakup after the pinch, are discussed in literature.[26] These so-called suprathermal Sn ions are accelerated along the discharge axis and may scatter on ions or atoms or on the electrode surfaces. In order to validate which of these processes play part in the production of the high-energy ion beam, future experiments are planned.

[1]V. Banine, O. Frijns, and G. Swinkels, International Extreme Ultraviolet Lithography (EUVL) Symposium, Sapporo, Japan, 28–31 October 2007 (unpublished).
[2]H. Meiling, S. Lok, B. Hultermans, E. van Setten, B. Pierson, K. Cummings, C. Wagner, and N. Harned, International Extreme Ultraviolet Lithography (EUVL) Symposium, Lake Tahoe, CA, 28 September–1 October 2008 (unpublished).
[3]M. Corthout, M. Yoshioka, *et al.*, International Extreme Ultraviolet Lithography (EUVL) Symposium, Lake Tahoe, CA, 28 September–1 October 2008 (unpublished).
[4]E. Wagenaars, A. Mader, K. Bermann, J. Jonkers, and W. Neff, IEEE Trans. Plasma Sci. **36**, 1280 (2008).
[5]J. Benschop, V. Banine, S. Lok, and E. Loopstra, J. Vac. Sci. Technol. B **26**, 2204 (2008).
[6]V. Medvedev, R. Gayzoe, V. Krivtsun, V. Ivanov, and K. Koshelev, *Comparison of Spectra of Accelerated Ions Produced by LPP and DPP*, 23rd Symposium on Plasma Physics and Technology, Prague, Czech Republic, 16–19 June 2008 (unpublished).
[7]M. Murakami, Y. G. Kang, K. Nishihara, S. Fujioka, and H. Nishimura, Phys. Plasmas **12**, 062706 (2005).
[8]G. Zukakishvili, V. Krivtsun, V. Gomozov, V. Ivanov, I. Kharkin, D. Glushkov, and K. Koshelev, *Generation of Fast Ions in Vacuum Sparks*, 23rd Symposium on Plasma Physics and Technology, Prague, Czech Republic, 16–19 June 2008 (unpublished).
[9]K. N. Koshelev and N. R. Pereira, J. Appl. Phys. **69**, R21 (1991).
[10]E. R. Kieft, J. J. A. M. van der Mullen, G. M. W. Kroesen, V. Banine, and K. N. Koshelev, Phys. Rev. E **71**, 026409 (2005).
[11]E. R. Kieft, J. J. A. M. van der Mullen, and V. Banine, Phys. Rev. E **72**, 026415 (2005).
[12]G. Zukakishvili (private communication).
[13]A. Hughes and V. Rojansky, Phys. Rev. **34**, 284 (1929).
[14]J. E. Monahan, J. Appl. Phys. **24**, 434 (1953).
[15]D. Roy and J. D. Carette, Appl. Phys. Lett. **16**, 413 (1970).
[16]D. Roy and J. D. Carette, Rev. Sci. Instrum. **42**, 1122 (1971).
[17]M. Arnow, J. Phys. E **9**, 372 (1976).
[18]B. Brehm, J. Grosser, T. Ruscheinski, and M. Zimmer, Meas. Sci. Technol. **6**, 953 (1995).
[19]H. C. Straub, M. A. Mangan, B. G. Lindsay, K. A. Smith, and R. F. Stebbings, Rev. Sci. Instrum. **70**, 4238 (1999).
[20]M. Krems, J. Zirbel, M. Thomason, and R. D. DuBois, Rev. Sci. Instrum. **76**, 093305 (2005).
[21]J. S. Pearlman, Rev. Sci. Instrum. **48**, 1064 (1977).
[22]G. Gerdin, W. Stygar, and F. Venneri, J. Appl. Phys. **52**, 3269 (1981).
[23]See, e.g., http://www.kimballphysics.com/detectors/detect_prod.htm.
[24]T. S. Green, Plasma Phys. **12**, 877 (1970).
[25]R. Janmohamed, G. Redman, and Y. Y. Tsui, IEEE Trans. Plasma Sci. **34**, 455 (2006).
[26]D. D. Ryutov, M. S. Derzon, and M. K. Matzen, Rev. Mod. Phys. **72**, 167 (2000).
[27]P. Mora, Phys. Rev. Lett. **90**, 185002 (2003).
[28]K. N. Koshelev, H. J. Kunze, R. Gayazov, V. Gomozov, V. V. Ivanov, V. G. Koloshnikov, E. D. Korop, V. Krivtsun, Yu. V. Sidelnikov, O. Yakushev, and G. G. Zukakishvili, in *EUV Sources for Lithography*, edited by V. Bakshi (SPIE, Bellingham, WA, 2006), Chap. 6.

Downloaded 27 Apr 2010 to 131.155.108.152. Redistribution subject to AIP license or copyright; see http://jap.aip.org/jap/copyright.jsp